A STUDY OF CP-VIOLATION IN B^0 DECAYS

Nobu Katayama*
Institute of Particle and Nuclear Studies
High Energy Accelerator Research Organization
Oho 1–1, Tsukuba-shi, 305–0801, Japan

Representing the Belle Collaboration

ABSTRACT

We present a preliminary measurement of time-dependent CP asymmetries in B^0 decays using the Belle detector at the KEKB asymmetric e^+e^- collider. The data sample consists of $6.2\,\mathrm{fb}^{-1}$ collected at the $\Upsilon(4S)$ resonance. One of the neutral B mesons is fully reconstructed via its decay to a CP eigenstate. The flavor of the other B meson is tagged mainly with the charge of identified leptons and kaons. The time interval between the two decays is determined from the distance between the decay vertices. A maximum likelihood method is used to extract $\sin 2\phi_1$ from the asymmetry in the time interval distribution. We present a preliminary result of $\sin 2\phi_1 = 0.45^{+0.43}_{-0.44}(stat)^{+0.07}_{-0.09}(syst)$.

*E-mail address:nobu.katayama@kek.jp

1 Introduction

The CP violating effects have been observed in K_L decay.[1] Kobayashi and Maskawa proposed an elegant explanation of these effects in the three-generation Standard Model.[2] In their model, CP violation is a consequence of the complex phases in the quark mixing matrix,

$$\begin{pmatrix} V_{ud} & V_{us} & V_{ub} \\ V_{cd} & V_{cs} & V_{cb} \\ V_{td} & V_{ts} & V_{tb} \end{pmatrix}$$

The nontrivial complex phases are conventionally assigned to the furthest off-diagonal elements V_{ub} and V_{td}. Sanda and Carter pointed out that the KM model contained the possibility of rather sizable CP violating asymmetries in certain decay modes of the B mesons.[3]

Unitarity of the KM matrix implies that $\sum_i V_{ij} V_{ik}^* = \delta_{jk}$, which gives the following relation involving V_{ub} and V_{td}:

$$V_{td}V_{tb}^* + V_{cd}V_{cb}^* + V_{ud}V_{ub}^* = 0.$$

This relation can be expressed as a closed triangle in the complex plane. The three interior angles of this triangle (the Unitarity Triangle) are defined as:

$$\phi_1 \equiv \arg\frac{V_{cd}V_{cb}^*}{V_{td}V_{tb}^*}, \qquad \phi_2 \equiv \arg\frac{V_{ud}V_{ub}^*}{V_{td}V_{tb}^*}, \qquad \phi_3 \equiv \arg\frac{V_{cd}V_{cb}^*}{V_{ud}V_{ub}^*}.$$

In e^+e^- storage rings operating at the $\Upsilon(4S)$ resonance, a $B^0\bar{B}^0$ pair produced in a decay of the $\Upsilon(4S)$ remains in a coherent P-wave state until one of the B mesons decays. In this state, when a neutral B meson decays into a CP eigenstate f, there is an interference between two amplitudes, $A(B^0 \to f)$ and $A(B^0 \to \bar{B}^0 \to f)$, which gives a time-dependent CP asymmetry shown by

$$A_{CP}(\Delta t) = \frac{R(B^0 \to f;\ \Delta t) - R(\bar{B}^0 \to f;\ \Delta t)}{R(B^0 \to f;\ \Delta t) + R(\bar{B}^0 \to f;\ \Delta t)} = \eta_f \sin 2\phi_{CP} \sin(\Delta m_d \Delta t),$$

where η_f is the CP eigenvalue of f, Δm_d is the mass difference between the two B^0 mass eigenstates and Δt is the proper time difference between two B meson decays, *i.e.* $\Delta t = t_2 - t_1$, where t_1 and t_2 are the proper time for the B^0 and $\bar{B}^0$ decays, respectively. The angle ϕ_{CP} is the phase difference between the two interfering amplitudes, which is directly related to the interior angles of the unitarity triangle. It can be shown that ϕ_{CP} is equal to ϕ_1 when $J/\psi K_S$, or another decay mode that arises from $b \to c\bar{c}s$, is used as the CP eigenstate f. This asymmetry vanishes in the time integrated rate. This is the motivation for the asymmetric beam energies in the B factories.[4]

At an asymmetric collider, Δt can be deduced from the distance, Δz between the two B^0 decay vertices along the axis of the boost, $\Delta t \approx \Delta z/(c\beta\gamma)$, where $\beta\gamma$ is the Lorentz boost factor from the asymmetric beam energies. The CP asymmetry is thus observed as an asymmetry in the distribution of the difference between the proper decay distances of the two B mesons produced in the decay of $\Upsilon(4S)$, one B decaying to the CP eigenstate and another to any final state with its flavor tagged.

2 KEKB and Belle

2.1 The KEKB asymmetric e^+e^- collider

KEKB[5] is an asymmetric e^+e^- collider of 3 km circumference, consisting of 8 GeV e^- and 3.5 GeV e^+ storage rings and an injection linear accelerator for them. The collider has one interaction point (IP) where the e^+ and e^- beams collide with a finite crossing angle of 22 mrad. The instantaneous luminosity of the KEKB collider reached $2.04\times10^{33}/\mathrm{cm}^2/\mathrm{sec}$ in July 2000. At KEKB, the average boost of the $\Upsilon(4S)$ and its daughter B mesons is $\beta\gamma \approx 0.425$ in the laboratory frame. The average distance of the two decay vertices of the B mesons is approximately 200μm.

2.2 The Belle detector

The Belle experiment at KEKB has recently completed a successful first year of operation. The Belle detector collected a total integrated luminosity of $6.8\,\mathrm{fb}^{-1}$, of which $6.2\,\mathrm{fb}^{-1}$ are taken on the $\Upsilon(4S)$ resonance and $0.6\,\mathrm{fb}^{-1}$ at 60 MeV below the resonance. A detailed description of the Belle detector can be found elsewhere.[6]

2.2.1 Charged particle tracking system

Charged particles are detected and their momenta measured by a three-layer, double sided silicon vertex detector (SVD) and a fifty layer small-cell cylindrical drift chamber (CDC). Eighteen layers of the CDC are inclined at small angle in order to provide three-dimensional reconstruction of charged particle trajectories. The CDC is operated with a $He(50\%)+C_2H_6(50\%)$ mixture to ensure a good momentum resolution in particular for low momentum particles. The CDC covers the polar angle region between 17 and 150 degrees in the laboratory frame, where polar angle is measured with respect to the opposite direction of the positron beam. The CDC also provides the measurement of energy loss for charged particles with a resolution of $\sigma(dE/dx)$= 6.9%. The vertex measurement is provided by the SVD. The double-sided silicon strip detectors (DSSD) are arranged in barrel configuration and cover 86% of solid angle. The three layers are at radii of 3.0, 4.5 and 6.0 cm, respectively. Each DSSD consists of 1280 ϕ strips with 25μm pitch, and 640 z strips with 84μm pitch. The resolutions of the impact parameters in the plane transverse to the beam axis (xy plane) and along the beam axis (z axis) are measured to be σ_{xy}=21$\oplus$69/$(p\beta\sin^{3/2}\theta)\mu$m and σ_z=41$\oplus$48/$(p\beta\sin^{5/2}\theta)\mu$m, respectively, where p is momentum of the particle measured in GeV/c and θ is the polar angle of the direction of the particle. The transverse momentum resolution is $\sigma_{p_t}/p_t = 0.0019\, p_t \oplus 0.0034$ where p_t is measured in GeV/c. The beampipe is made of double-wall beryllium of 2.3 cm radius and 1 mm thick. The tracking system is situated in a 1.5 T solenoidal magnetic field.

2.2.2 Kaon identification system

The charged kaon identification is provided by the dE/dx measurements in the CDC, aerogel Cherenkov counters (ACC) and time-of-flight scintillation counters (TOF). The ACC consists of 1188 aerogel blocks with the refractive indices between 1.01 and 1.03 depending on the polar angle. The Cherenkov light is detected by fine-mesh photomultipliers directly attached to the aerogel blocks. The effective number of photoelectrons is approximately 6 for $\beta = 1$ particles. The TOF consists of 128 plastic scintillators viewed by fine-mesh photomultipliers on both ends. The time resolution is 95 psec (rms), which provides $\pi^\pm/K^\pm$ separation up to 1.2 GeV.

The charged kaon identification probabilities are calculated from the combined response of the three systems. The efficiency for $K^\pm$ is $\approx$80% while the charged pion fake rate as kaon is $\approx$10% for momentum up to 3.5 GeV/c.

2.2.3 Photon detection system

The electromagnetic calorimetry (ECL) is provided by an array of 8736 CsI(Tl) crystals of 16.1 radiation lengths. The ECL covers the same angular region as the CDC. The photon energy resolution is measured, in a beam test, to be $\sigma_E/E = (1.3 \oplus 0.07/E \oplus 0.8/E^{1/4})\%$, where E is measured in GeV. Neutral pions are detected via their decay to $\gamma\gamma$. The π^0 mass resolution varies slowly with their energy, averaging $\sigma_{m_{\pi^0}}$ of $4.9\,\mathrm{MeV/c^2}$. With a $\pm 3\sigma$ mass selection requirement, the overall detection efficiency, including geometric acceptance, for π^0s in the $B\bar{B}$ events is 40%.

2.2.4 Lepton identification system

Electron identification is based on the dE/dx measurements in the CDC, the response of the ACC, and the position, shape and energy deposit of CsI clusters that have been associated with the electron trajectory in the charged particle tracking system (CDC and SVD). Likelihood functions as electrons and non-electrons are constructed to discriminate between them. This is above 90% efficient for electrons and has a ≈0.5% fake probability for charged hadrons with momenta above 1 GeV/c.

In the return yoke of the solenoidal magnetic field are instrumented 14 layers of resistive plate counters (KLM) between 4.7 cm-thick iron plates. The KLM detects muons and K_Ls in the angular region of $20^\circ < \theta < 155^\circ$. The overall muon identification efficiency is above 90% for muons with momentum above 1.0 GeV/c with a pion fake probability of 4%.

2.2.5 K_L detection

K_L mesons are identified by the presence of energy deposits originating from hadronic interactions of the K_L in the CsI and/or iron. If there are CsI clusters associated with a candidate K_L, its direction is determined from the energy-weighted center of gravity of the energy deposit of the CsI counter alone. Otherwise, the direction is determined from the average position of the associated KLM hits. The angular resolution of the K_L direction is estimated to be $\approx 1.5^\circ$ and $\approx 3^\circ$ with and without associated CsI clusters, respectively.

2.3 Hadronic event selection

The hadronic events are selected by requiring:

- At least three "good" charged tracks be coming from the IP; where a "good" track has a minimum transverse momentum of 0.1 GeV/c and originates within 2.0 cm and 4.0 cm of the average IP in the xy plane and along the z axis.
- At least two "good" neutral clusters be observed in the barrel region of the calorimeter, where a "good" cluster is detected in the good acceptance region with an energy deposit greater than 0.1 GeV, and no charged tracks are associated with the cluster.
- A sum of all cluster energies, after a boost back into to the center-of-mass frame, and assuming they are deposited by massless particles, to be between 10% and 80% of the center-of-mass energy.
- The total visible energy, computed as the sum of the "good" tracks assuming pions and the "good" clusters in the center-of-mass frame, exceeds 20% of the center-of-mass energy.
- The absolute value of the momentum balance in z, calculated in the center-of-mass frame, to be less than 50% of the center-of-mass energy.
- The event vertex reconstructed from the "good" tracks, to be within 1.5 cm and 3.5 cm of the IP in the xy plane and along the z axis, respectively.

From Monte Carlo simulation studies, the efficiency to retain $B\bar{B}$ events is estimated to be 92.5%. For $B \to J/\psi X$ events, the efficiency is estimated to be 99.4%.

We applied slightly tighter selection criteria for the data in the earlier part of the data taking period. The tighter set of cuts gives a few percent lower efficiency for the J/ψ events.

Events passing the hadronic event selection criteria and satisfying $H_2/H_0 \leq 0.5$, where H_2 and H_0 are the second and 0-th Fox-Wolfram moments, are used in the subsequent analysis.

3 Analysis Procedures

The measurement of the CP violation asymmetry has four major steps: (1) selection of the decay of one of the neutral B mesons into a CP eigenstate, (2) determination of the flavor of the other B meson, (3) measurement of the distance Δz between the two B^0 decay vertices, and (4) extraction of the amplitude of the CP asymmetry and the value of $\sin 2\phi_1$ using an unbinned maximum likelihood fit.

We would like to determine, whenever possible, resolutions, efficiencies and wrong-tag fractions from the data. The measurements of B lifetimes and the neutral B meson mixing parameter have been made and are discussed in the following sections, as they have the same above-described steps in the analyses.

3.1 Reconstruction of the CP eigenstates

We reconstruct B^0 decays to the following CP eigenstates; $J/\psi K_S, \psi(2S)K_S, \chi_{c1}K_S$ for $CP = -1$ states and $J/\psi\pi^0, J/\psi K_L$ for $CP = +1$ states.

3.1.1 Selection of J/ψ, $\psi(2S)$, χ_{c1} and K_S

The J/ψ and $\psi(2S)$ mesons are reconstructed via their decays to $\mu^+\mu^-$ and e^+e^-. For the $J/\psi \to \mu^+\mu^-$ candidates, at least one track is positively identified as a muon by the KLM and the other is either positively identified as a muon or has a CsI energy deposit that is consistent with that of a minimum ionizing particle. For the $J/\psi \to e^+e^-$ candidates, at least one track is positively identified as an electron and the other track has an energy deposit in the CDC dE/dx system or the CsI calorimetry system that is consistent with that of an electron. For the dielectron candidates, we correct for final state radiation or Bremsstrahlung in the inner parts the detector by including the four-momentum of every photon detected within 0.05 radian of the original electron in the invariant mass calculation. The invariant mass distributions for the $J/\psi \to \mu^+\mu^-$ candidates, the $J/\psi \to e^+e^-$ candidates, and the $\psi(2S) \to \mu^+\mu^-, e^+e^-$ candidates are shown in Figures 1(a), (b) and (c), respectively. The $\psi(2S)$ is also reconstructed via its decay to $J/\psi\pi^+\pi^-, J/\psi \to \mu^+\mu^-, e^+e^-$ and the χ_{c1} via the mode $J/\psi\gamma$. Figures 2(a) and (b) show the mass difference distributions, $M_{\ell^+\ell^-\pi^+\pi^-} - M_{\ell^+\ell^-}$ and $M_{\ell^+\ell^-\gamma} - M_{\ell^+\ell^-}$.

For the $K_S \to \pi^+\pi^-$ candidates, the oppositely charged track pairs are required

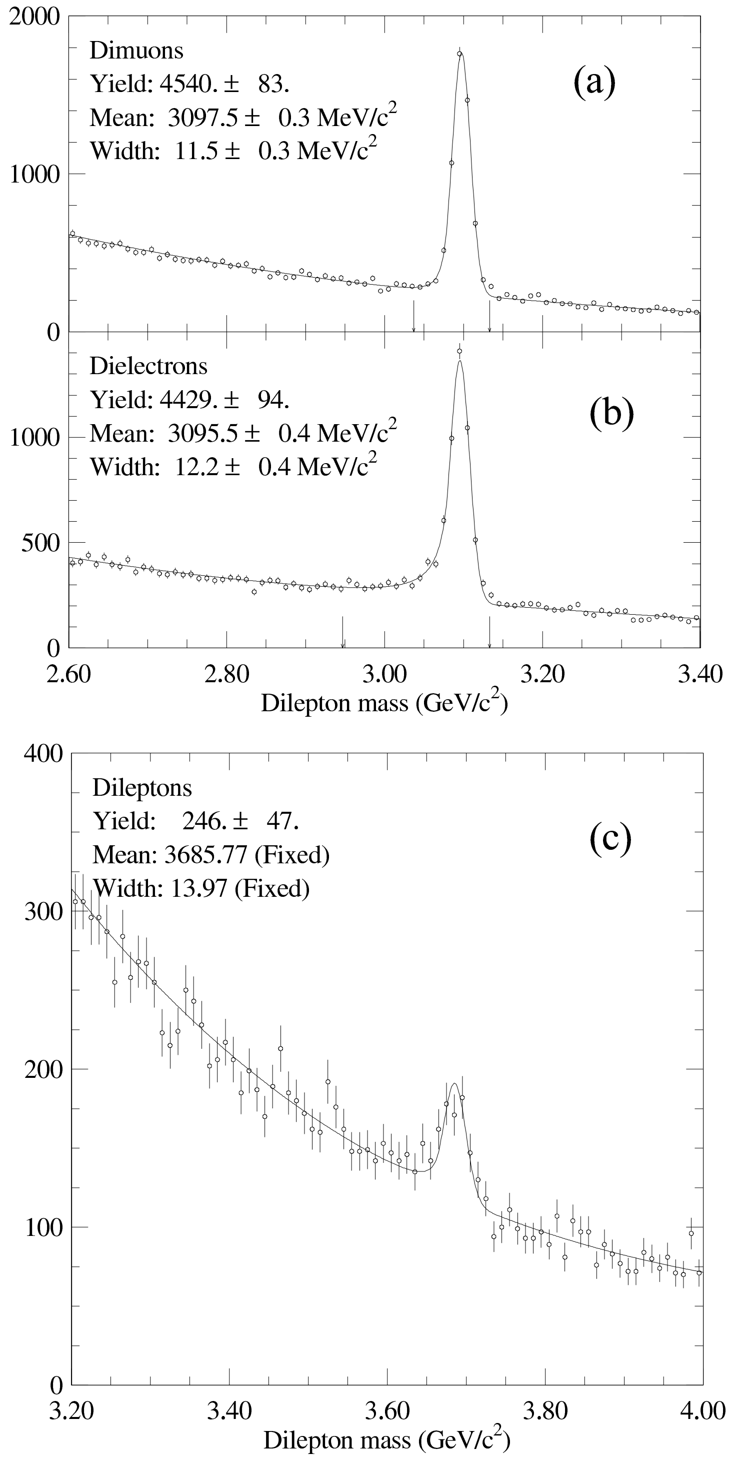

Fig. 1. The invariant mass distributions for (a) $J/\psi \to \mu^+\mu^-$, (b) $J/\psi \to e^+e^-$ and (c) $\psi(2S) \to \mu^+\mu^-$ and e^+e^-.

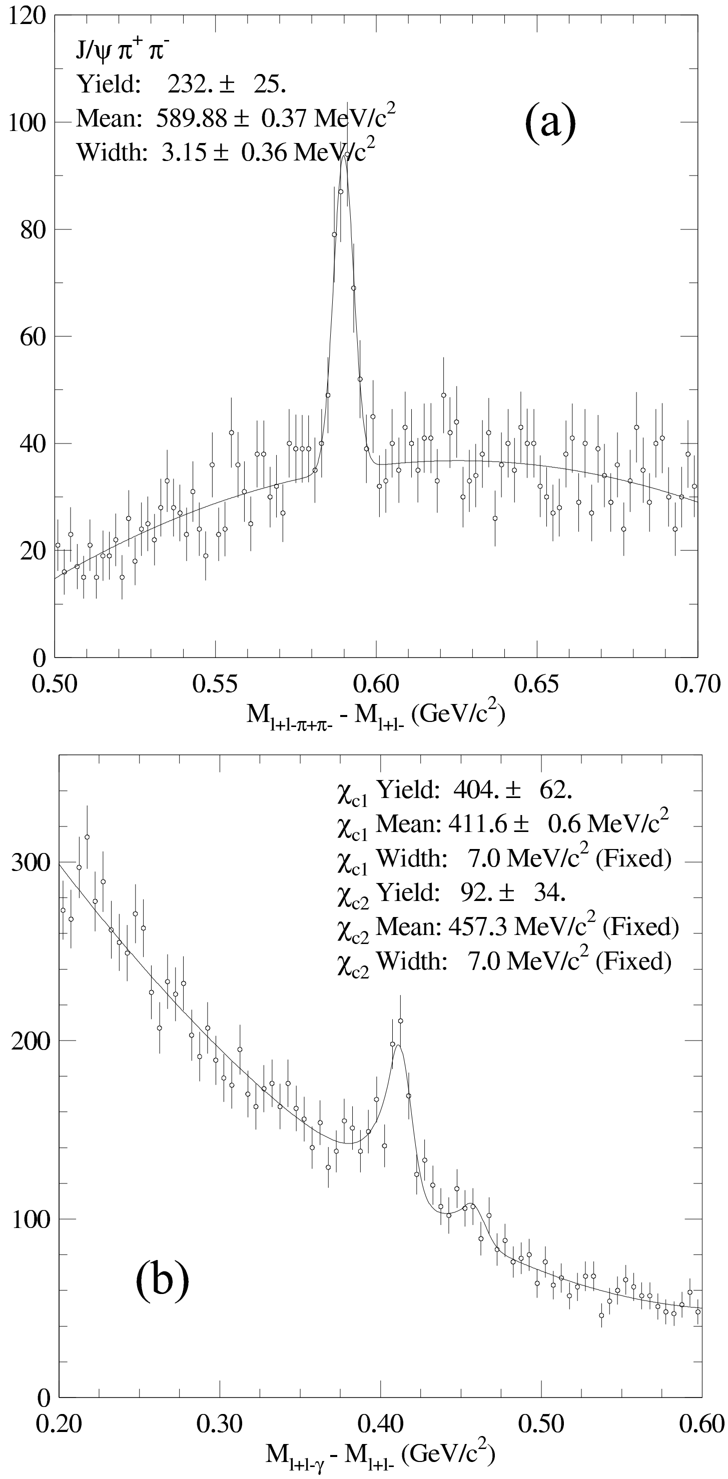

Fig. 2. The invariant mass difference distributions for (a) $M_{\ell^+\ell^-\pi^+\pi^-} - M_{\ell^+\ell^-}$ and (b) $M_{\ell^+\ell^-\gamma} - M_{\ell^+\ell^-}$.

to have an invariant mass between 482 and 514 MeV/c^2, which corresponds to $\pm 3\sigma$ around the K_S mass peak. The $K_S \to \pi^0\pi^0$ decay candidates are also used for reconstructing the $J/\psi K_S$ decay channel. The K_S are selected among photons with a minimum energy of 50 MeV and 200 MeV in the barrel and end-cap regions, respectively, by requiring, assuming that the K_S decayed at the IP, (a) a minimum π^0 momentum of 100 MeV/c, (b) $118 < M_{\gamma\gamma} < 150$ MeV/c^2, and (c) $300 < M_{\pi^0\pi^0} < 1000$ MeV/c^2. For each candidate, we determine the most probable K_S decay point by minimizing the sum of the χ^2 values from constraining each photon pair to π^0 invariant mass, while varying the K_S decay point along the K_S flight direction that is defined by the sum of four photon momenta and the IP. We then recalculate the invariant masses of the photon pairs and the π^0 and require the recalculated K_S mass to be in between 470 and 520 MeV/c^2. For the $J/\psi\pi^0$ decay mode, the π^0 candidates are selected from photons with minimum energy of 100 MeV.

3.1.2 Selection of the B candidates

To identify reconstructed B meson decays we use the beam-constrained mass, $M_{beam} \equiv \sqrt{E_{beam}^2 - p_B^2}$ and the energy difference $\Delta E \equiv E_B - E_{beam}$, where E_{beam} is half of the center-of-mass energy and p_B and E_B are the B candidate's absolute three-momentum and energy calculated in the center-of-mass system. Figure 3 shows the M_{beam} distribution of the combined $B \to J/\psi K_S, K_S \to \pi^+\pi^-$; $J/\psi K_S, K_S \to \pi^0\pi^0$; $\psi(2S)K_S, K_S \to \pi^+\pi^-$; $\chi_{C1}K_S, K_S \to \pi^+\pi^-$; and $J/\psi\pi^0$ decay candidates, with a $\pm 3.5\sigma$ cut on $|\Delta E|$. The actual value of the cut varies with the decay mode; ± 40 MeV for modes with $K_S \to \pi^+\pi^-$ and ± 100 MeV for modes containing π^0s. All B meson candidates within 10 MeV from the mean of M_{beam} are considered as signal. Table 1 lists the number of signal B mesons, and the backgrounds which are estimated using the events lying outside of the signal region and from the full Monte Carlo simulation results.

3.1.3 Selection of $J/\psi K_L$

The $B^0 \to J/\psi K_L$ candidates are selected by requiring the J/ψ candidate momentum and the K_L direction to be consistent with the $B^0 \to J/\psi K_L$ two body decay hypothesis. After requiring the J/ψ momentum to be between 1.42 and 2.0 GeV/c in the center-of-mass frame, we calculate the momentum of the B

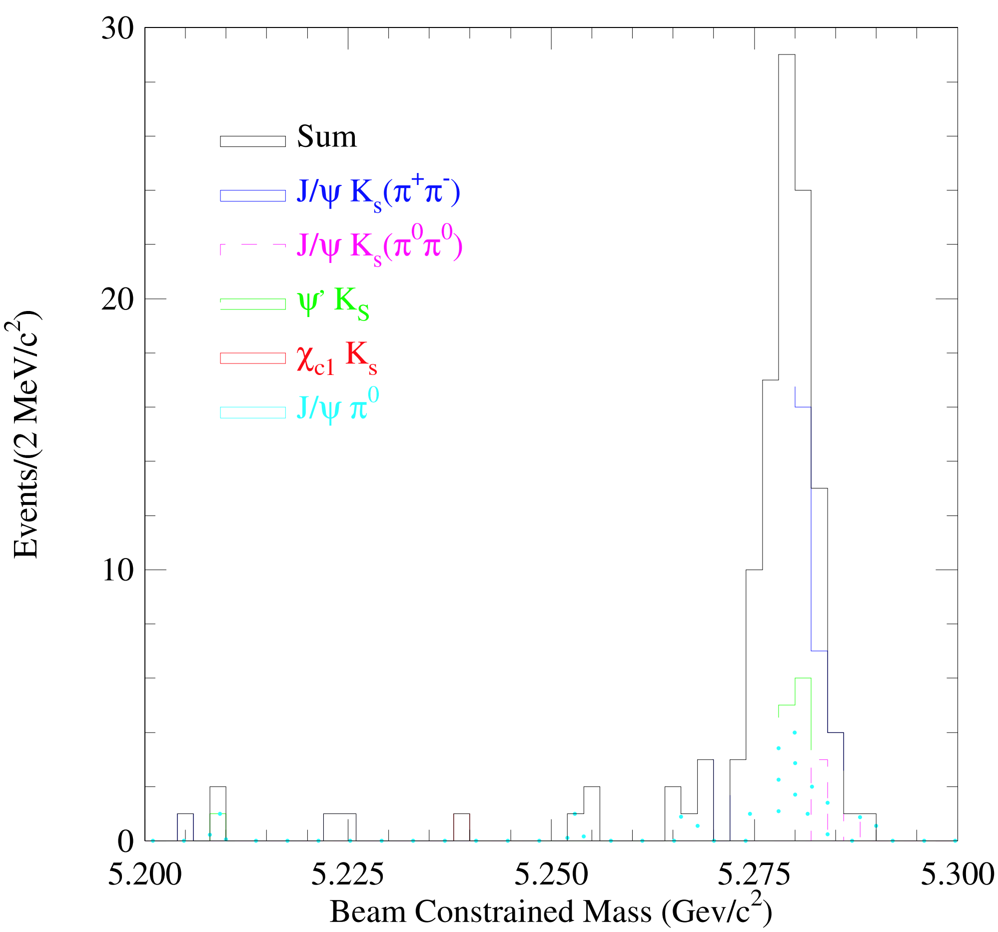

Fig. 3. The beam constrained mass distribution of the combined $B \to J/\psi K_S(\pi^+\pi^-), J/\psi K_S(\pi^0\pi^0), \psi(2S)K_S(\pi^+\pi^-), \chi_{C1}K_S(\pi^+\pi^-)$, and $J/\psi\pi^0$ decay candidates with a $\pm 3.5\sigma$ cut on $|\Delta E|$.

Table 1. Summary of the reconstructed CP eigenstates

Mode	N_{events}	$N_{background}$
$B \to J/\psi K_S,\ K_S \to \pi^+\pi^-$	70	3.4
$B \to J/\psi K_S,\ K_S \to \pi^0\pi^0$	4	0.3
$B \to \psi(2S) K_S,\ K_S \to \pi^+\pi^-,\ \psi(2S) \to \ell^+\ell^-$	5	0.2
$B \to \psi(2S) K_S,\ K_S \to \pi^+\pi^-,\ \psi(2S) \to J/\psi\pi^+\pi^-$	8	0.6
$B \to \chi_{C1} K_S,\ K_S \to \pi^+\pi^-$	5	0.75
$B \to J/\psi\pi^0$	10	1
Total	102	6.25

meson, p_B^*, using the K_L direction and the B meson mass. Figure 4 shows the p_B^* distribution. The p_B^* should be about 0.34 GeV/c for a true $B^0 \to J/\psi K_L$ candidate. Also shown are expected distributions of signal and background derived from the full Monte Carlo simulation studies. The background is found to be dominated by $B^0 \to J/\psi X$ events including $B^0 \to J/\psi K^{*0}, K^{*0} \to K_L\pi^0$ and $B^0 \to J/\psi$ non-resonant $K_L\pi^0$, which are a mixture of $CP = +1$ and $CP = -1$ eigenstates. There are 102 $J/\psi K_L$ candidates in the signal region, which is defined as $0.2 < p_B^* < 0.45\,\mathrm{GeV/c}$. By fitting the data with the expected signal and background shapes, we estimate that there are 48 background events in the signal region, of which 8 events are from $B^0 \to J/\psi K^{*0}, K^{*0} \to K_L\pi^0$ and $B^0 \to J/\psi+$ non-resonant $K_L\pi^0$.

3.2 Flavor tagging

Each event with a CP eigenstate decay candidate is classified as a B^0 or $\bar{B}^0$ tag if the rest of the event contains a signature that is specific to B^0 or $\bar{B}^0$ decays. The rest of the event is defined as the event with the daughter charged and neutral tracks of the CP eigenstate decay candidate removed.

For the tagging methods, we use the sign of the primary lepton in semi-leptonic B^0 decay, and the kaon charge which is the signature of a cascade decay $b \to c \to s$. We define the charged and neutral tracks used in reconstruction of the CP eigenstate decay mode as “CP-side” tracks, and the rest of the tracks as “tag-side” tracks. We assign the B-flavor for the tag-side B-meson (B_{tag}) using the following criteria:

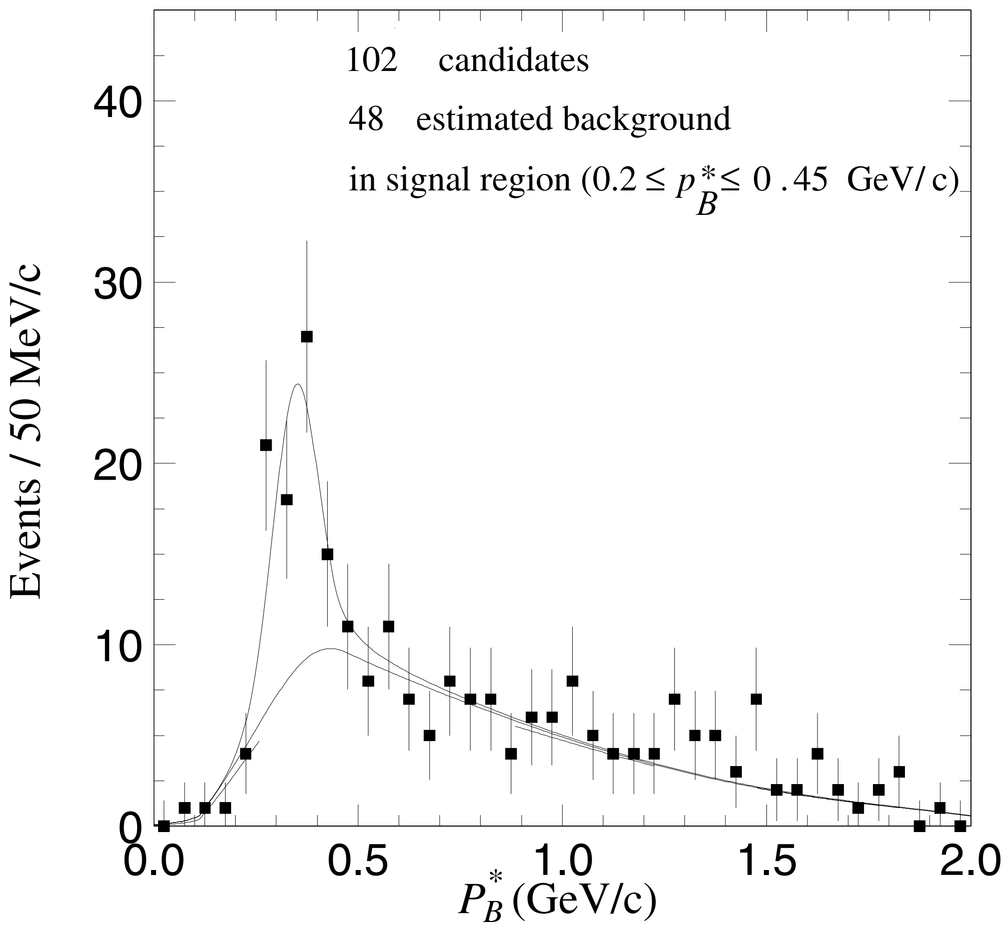

Fig. 4. The p_B^* distribution for $J/\psi K_L$ candidates with the results of the fit. The upper solid line is a sum of the signal and backgrounds. The total background (lower solid line) is divided into those coming from $J/\psi K^{*0}$, $K^{*0} \to K_L \pi^0$ and $J/\psi + \mathrm{non-resonant}\ K_L\pi^0$, and those coming from all other sources (below the dotted line).

1. High momentum lepton: If B_{tag} contains a high momentum lepton ($p^*_{\ell epton} > 1.1$ GeV/c for both electrons and muons) which comes from the semileptonic decay of $B_{\rm tag}$. $B_{\rm tag} = B^0$ for ℓ^+ and $B_{\rm tag} = \bar{B}^0$ for ℓ^- are assigned. We first test whether the event contains an electron. If the event fails the test then we test whether it contains a muon. No flavor is assigned when two or more high momentum electrons or muons satisfy the criteria.

2. Charged kaon: If B_{tag} does not contain any high momentum lepton, the sum of the charges of all identified kaons in B_{tag}, Q_K is computed. $B_{\rm tag} = B^0$ for $Q_K > 0$ and $B_{\rm tag} = \bar{B}^0$ for $Q_K < 0$ are assigned.

For the above flavor tagging methods, we use the tag-side tracks satisfying $|dr| < 3$cm and $|dz| < 4$cm. We require the lepton identification probability be greater than 0.5 for electrons and 0.8 for muons, where the probabilities for electron and muon identification are calculated as mentioned previously. For charged kaons, we require the particle identification probability ratio be greater than 0.9 for K/π, less than 0.6 for e/K, and less than 0.7 for p$/K$.

The efficiency and wrong-tag fraction are measured using exclusively reconstructed $B \to D^{(*)}\ell\nu$ events from the same data sample. Here, we define

- Tagging efficiency: $\epsilon_{tag} = N_{tag}/N_{rec}$, where N_{rec} and N_{tag} are number of reconstructed and tagged CP events, respectively.

- Wrong-tag fraction: $\omega =$ (number of wrongly tagged events)/(total number of tagged events)

3.2.1 Measurement of wrong-tag fraction from B^0 mixing

Taking into account the wrong-tag farction, the time evolution of the opposite flavor (OF) and same flavor (SF) neutral B-meson pair is given as

$$\begin{aligned}
\mathcal{P}_{OF}(\Delta t) &\propto 1 + (1-2\omega)\cos(\Delta m_d \Delta t), \\
\mathcal{P}_{SF}(\Delta t) &\propto 1 - (1-2\omega)\cos(\Delta m_d \Delta t).
\end{aligned}$$

The wrong-tag fraction determines the oscillation amplitude of the OF-SF asymmetry,

$$A_{mix} = \frac{\mathcal{P}_{OF} - \mathcal{P}_{SF}}{\mathcal{P}_{OF} + \mathcal{P}_{SF}} = (1-2\omega)\cos(\Delta m_d \Delta t).$$

We fit the time evolution of the OF and SF events simultaneously and measure the wrong-tag fraction.

We use the following decay modes:

- $B^0 \to D^{*-}\ell^+\nu$, $D^{*-} \to \bar{D}^0\pi^-$
  - $\bar{D}^0 \to K^+\pi^-$
  - $\bar{D}^0 \to K^+\pi^-\pi^0$
  - $\bar{D}^0 \to K^+\pi^+\pi^-\pi^-$
- $B^0 \to D^-\ell^+\nu$, $D^- \to K^+\pi^-\pi^-$

The vertex position of the $D^{(*)}\ell\nu$ is determined in the following way. First, we fit the D meson vertex using the K and π tracks, where the $K\pi$ invariant mass is constrained to the world average D mass. For the $K\pi\pi^0$ mode, the D mass constraint is not used. Then, the ℓ and D tracks are fit to form the B vertex. The slow pion track from the D^* is not used in the fit, as it does not help to improve the B vertex resolution.

We apply the flavor tagging methods described above to the tag-side, treating the tracks used in the reconstruction of the $D^{(*)}\ell\nu$ decay as the CP-side tracks. To reconstruct the tag-side vertex position of the mixing events, we use the same method as in an analysis to be described in detail later.

We measure the wrong-tag fraction together with the mixing parameter Δm_d by fitting the Δz distribution of the SF and OF events. Figure 5 shows the OF–SF asymmetries as a function of Δt for tagged $D^{*\mp}\ell^\pm\nu$ and $D^\mp\ell^\pm\nu$ events together with the results of the fit.

The results of the fit are

$$\begin{aligned}
\Delta m_d &= 0.488 \pm 0.026\,\mathrm{ps}^{-1}, \\
\omega_{\ell epton} &= 0.071 \pm 0.019(stat), \\
\omega_K &= 0.199 \pm 0.021(stat).
\end{aligned}$$

Using the same $D^{(*)}\ell\nu$ sample, the tagging efficiencies are also determined.

$$\begin{aligned}
\epsilon_{\ell epton} &= 0.142 \pm 0.005(stat) \pm 0.020(sys), \\
\epsilon_K &= 0.279 \pm 0.007(stat) \pm 0.041(sys).
\end{aligned}$$

We estimate the systematic errors of the ω's due to uncertainties in the response function, backgrounds, and Monte Carlo parameters used in the fit. The total

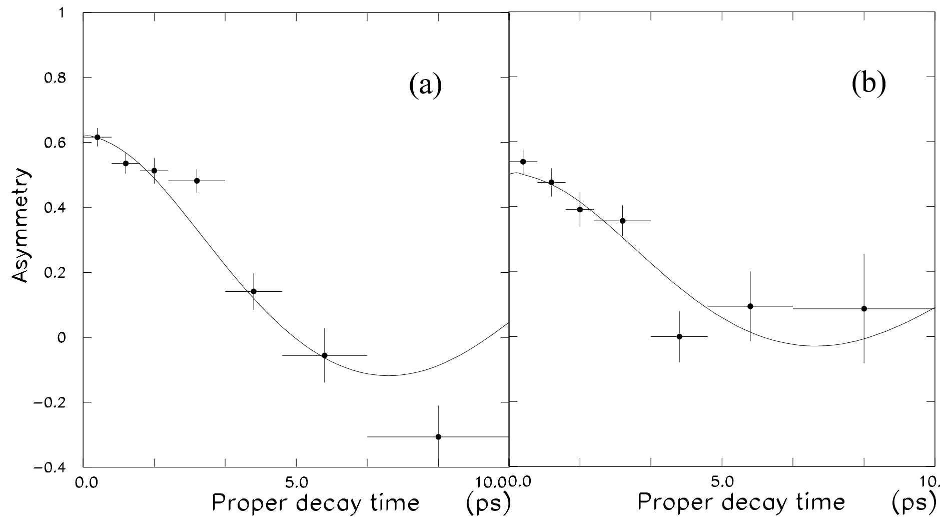

Fig. 5. The $B^0 - \bar{B}^0$ mixing asymmetry as a function of the proper time interval Δt between the two neutral B meson decays, (a) for $D^*\ell$, (b) for $D^+\ell$ decays. Also shown are the results of the fit.

systematic error from these sources are ± 0.018 and ± 0.032 for $\omega_{\ell epton}$ and ω_K, respectively.

The wrong-tag fraction is also measured using the time-integrated number of the OF and SF events in the $D^{(*)\mp}\ell^\pm\nu$ sample. Taking into account the B^0-$\bar{B}^0$ mixing effect, ω is determined by the equations

$$\omega = \frac{\chi_{obs} - \chi_d}{1 - 2\chi_d}, \qquad \chi_d = \frac{\tau_{B^0}^2 \Delta m_d^2}{2(1 + \tau_{B^0}^2 \Delta m_d^2)}.$$

where $\chi_{obs} = N_{SF}/(N_{OF} + N_{SF})$. Using $\chi_d = 0.172 \pm 0.010$, we find that both results are consistent within errors.

As a further systematic check, we obtain the wrong-tag fractions in the $B^\pm \to J/\psi K^\pm$ events. Since $B^\pm$ does not mix and the $B^\pm \to J/\psi K^\pm$ sample is almost free from background, we can measure the wrong-tag fractions with small systematic errors. On the other hand, ω's for $B^\pm$ can be different from those of B^0 because the decay modes are different. For example, D^0 and $D^\pm$ inclusive production fractions are different. Monte Carlo simulation studies show ω's of $B^\pm$ are 2 to 3% smaller than those of B^0. We measure $\omega_{\ell epton}^\pm = 0.026 \pm 0.025(stat)$ and $\omega_K^\pm = 0.129 \pm 0.036(stat)$. We observe a larger difference between B^0 and $B^\pm$ ωs than that from the Monte Carlo simulation studies.

Based on the above studies, we conservatively take the difference between the measured ω's for B^0 and $B^\pm$ as the systematic errors on the ω's, and use in the following analysis:

$$\begin{aligned}\omega_{\ell epton} &= 0.071 \pm 0.045(total), \\ \omega_K &= 0.199 \pm 0.070(total).\end{aligned}$$

The results are summarized in Table 2 for the data and in Table 3 for the Monte Carlo simulation results.

Table 2. Summary of the tagging efficiencies (ϵ_{tag}), wrong-tag fractions (ω_{tag}), and effective tagging efficiencies (ϵ_{eff}) for the data.

	mode	ϵ_{tag} (data)	ω_{tag} (data)	ϵ_{eff} (data)
B^0	lepton	0.142 ± 0.021	0.071 ± 0.045	0.105 ± 0.027
	kaon	0.279 ± 0.042	0.199 ± 0.070	0.101 ± 0.049
	Total	0.421 ± 0.047	0.150 ± 0.051	0.206 ± 0.056
$B^\pm$	lepton	0.127 ± 0.019	0.026 ± 0.025	0.114 ± 0.021
	kaon	0.282 ± 0.026	0.129 ± 0.036	0.155 ± 0.033
	Total	0.409 ± 0.032	0.095 ± 0.033	0.269 ± 0.039

Table 3. Summary of the tagging efficiencies (ϵ_{tag}), wrong-tag fractions (ω_{tag}), and effective tagging efficiencies (ϵ_{eff}) from the Monte Carlo simulation studies.

	mode	ϵ_{tag} (MC)	ω_{tag} (MC)	ϵ_{eff} (MC)
B^0	lepton	0.123	0.088	0.084
	kaon	0.275	0.161	0.127
	Total	0.398	0.138	0.201
$B^\pm$	lepton	0.124	0.088	0.084
	kaon	0.291	0.126	0.162
	Total	0.414	0.108	0.246

In addition to the above tagging methods we also use the following tagging methods; (3) Mid-momentum lepton: If the event contains an identified lepton in the momentum range $0.6 < p^*_\ell < 1.1$ GeV/c, we use the missing momentum as an approximation of the ν momentum. If $|\mathbf{p}_\ell^* + \mathbf{p}_\nu^*| > 2.0$ GeV/c, we assume the event contains a $b \to c\ell\nu$ decay and assign its flavor based on the charge of the lepton as in the high momentum lepton method. (4) Soft pion: If the event contains a low momentum ($p^* < 200$MeV/c) charged track consistent with being a π from the $\bar{B}^0 \to D^{*+}$X, $D^{*+} \to D^0\pi^+$ decay chain, we assign the flavor of the event as $B^0(\bar{B}^0)$ for π^- (π^+). The effective tagging efficiency of the mid-momentum lepton (soft pion) method is estimated to be 0.50% (0.71%) from the Monte Carlo simulation studies and the wrong-tag fraction, 29% (34%).

The total effective tagging efficiency is estimated to be 21.8 $\pm$5.6%.

We find a total of 98 tagged events, of which 14 events were tagged by the high momentum e tag, 12 by high momentum μ, 48 by $K^\pm$, 3 by medium momentum e, 3 by medium momentum μ, and 18 by soft π. Table 4 summarizes the tagged events with reconstructed B candidates in various CP eigenstates.

Table 4. Summary of the tagged events with reconstructed CP eigenstates

Mode	N_{events}
$B \to J/\psi K_S, K_S \to \pi^+\pi^-$	40
$B \to J/\psi K_S, K_S \to \pi^0\pi^0$	4
$B \to \psi(2S) K_S, K_S \to \pi^+\pi^-, \psi(2S) \to \ell^+\ell^-$	2
$B \to \psi(2S) K_S, K_S \to \pi^+\pi^-, \psi(2S) \to J/\psi\pi^+\pi^-$	3
$B \to \chi_{C1} K_S, K_S \to \pi^+\pi^-$	3
$B \to J/\psi\pi^0$	4
$B \to J/\psi K_L$	42
Total	98

3.3 Vertexing

The proper time difference, Δt, is given by $\Delta t \simeq \Delta z/(c\beta\gamma)$ and Δz is the distance between the decay vertices of the two B mesons along the boost axis. The vertices for the CP-side are reconstructed from the leptons from the J/ψ, using the constraint that the tracks are coming from the IP profile smeared with finite B flight length in the r-ϕ plane. We use leptons only if there are sufficient numbers of SVD hits associated using the Kalman filtering technique; *i.e.* with both z and r-ϕ hits in at least one layer and with two or more z hits in total. The IP profile is calculated offline for every accelerator fill using hadronic events. The typical size of the IP profile is 100μm in the horizontal direction (x), 5μm in the vertical direction (y) and 3000μm in z. Because of the flat nature of the beam profile, the size in y is determined from the average luminosity, the beam current and the width of the measured vertex distribution in the x-coordinate. The efficiency of the vertex reconstruction is estimated to be 96% with $B^{\pm} \to J/\psi K^{\pm}$ and $B^0 \to J/\psi K^{*0}(\to K^{\pm}\pi^{\mp})$ events. The measured reconstruction efficiency is consistent with the expectation from the SVD acceptance and hit-matching efficiency.

The algorithm for tag-side vertex reconstruction is carefully chosen to minimize effects from long-lived particles, secondary vertices from charmed hadrons and poorly-reconstructed tracks. Among charged tracks remaining after the reconstruction of the CP-side, we use tracks with SVD hits (the same condition as that for the CP side) with an impact parameter with respect to the IP center of less than 1 mm in the r-ϕ plane, and less than 2 mm from the CP-side vertex in z. Tracks are also removed if they form a K_S candidate satisfying the K_S selection criteria and $|M_{K_S} - M_{\pi^+\pi^-}| < 15\,\mathrm{MeV}/c^2$; or if the track has a large tracking error in the z direction ($\sigma_z > 0.5$ mm); or if the distance between the track and the reconstructed CP-side vertex is too large ($\delta z > 1.8$ mm or $\delta r > 0.5$ mm). The remaining tracks are used to reconstruct the tag-side vertex with the IP constraint. The track with the largest χ^2 is removed from the fit if the reduced χ^2 (χ^2/ndf, where ndf is the number of degrees of freedom) of the vertex fit is greater than 20. In the case that such a track is the lepton which is used to tag the flavor of the event, however, we keep the lepton and remove the track with the second largest χ^2. This procedure is iterated until the reduced χ^2 becomes less than 20. If the number of remaining tracks becomes one, we impose a tighter requirement to ensure the quality of the vertex fitted with one track and the IP constraint; *i.e.* χ^2/ndf less than 6 and the momentum of the track greater than $0.6\,\mathrm{GeV}/c$. The reconstruction efficiency is measured to be 96% using $B^{\pm} \to J/\psi K^{\pm}$ and $B^0 \to J/\psi K^{*}(\to K^{\pm}\pi^{\mp})$ events.

3.3.1 Resolution function

The resolution function, $R_{sig}(\Delta t)$ is parameterized as the sum of two Gaussians:

$$R_{sig}(\Delta t) \;=\; (1-f_{tail})\frac{1}{\sqrt{2\pi}\sigma_{\Delta t}}e^{-\frac{(\Delta t-\mu_{\Delta t})^2}{2\sigma^2_{\Delta t}}} + f_{tail}\frac{1}{\sqrt{2\pi}\sigma^{\Delta t}_{tail}}e^{-\frac{(\Delta t-\mu^{\Delta t}_{tail})^2}{2(\sigma^{\Delta t}_{tail})^2}},$$

where f_{tail} is the fraction of the tail part of the resolution function, and $\sigma_{\Delta t}$, $\sigma^{\Delta t}_{tail}$, $\mu_{\Delta t}$ and $\mu^{\Delta t}_{tail}$ are the proper time difference resolutions and the shift in the mean value of the proper time difference for the main part and the tail part of the resolution function, respectively. f_{tail} is determined to be 0.04 ± 0.04 in the lifetime measurement using the $B \to \bar{D}^*\ell^+\nu$ sample with the same resolution function. $\mu_{\Delta t}$ and $\mu^{\Delta t}_{tail}$ originate from the shift in the mean value of the Δz measurement and are discussed below.

The proper time difference resolution, $\sigma_{\Delta t}$ (and $\sigma^{\Delta t}_{tail}$) is calculated event by event and is a convolution of the Δz resolution, $\sigma_{\Delta z}$, and the error due to the kinematic approximation ($\Delta t \approx \frac{\Delta z}{c(\beta\gamma)}$, $(\beta\gamma) = \frac{p_z(\Upsilon)}{m(\Upsilon)}$), σ_K:

$$\begin{aligned}\sigma_{\Delta t} &= \sqrt{(\frac{\sigma_{\Delta z}}{c(\beta\gamma)})^2 + \sigma_K^2},\\ \sigma^{\Delta t}_{tail} &= \sqrt{(\frac{\sigma^{\Delta z}_{tail}}{c(\beta\gamma)})^2 + (\sigma^K_{tail})^2}.\end{aligned}$$

The σ_K and σ^K_{tail} are determined to be $\sigma_K = 0.30 \pm 0.03\,\mathrm{ps}$ and $\sigma^K_{tail} = 0.0^{+0.4}_{-0.0}\,\mathrm{ps}$ from the Monte Carlo simulation studies as they are independent of the detector performance.

The Δz resolution $\sigma_{\Delta z}$ ($\sigma^{\Delta z}_{tail}$) is calculated from the vertex resolutions of the two B mesons, σ_z^{CP} and σ_z^{tag}:

$$\begin{aligned}\sigma^2_{\Delta z} &= S^2_{det}(\sigma_z^{CP})^2 + (S^2_{det} + S^2_{charm})(\sigma_z^{tag})^2\\ (\sigma^{\Delta z}_{tail})^2 &= (S^{det}_{tail})^2(\sigma_z^{CP})^2 + \{(S^{det}_{tail})^2 + (S^{charm}_{tail})^2\}(\sigma_z^{tag})^2\end{aligned}$$

where S_{charm} and S^{charm}_{tail} are scaling factors for the degradation of the vertex resolution of the tagging side B meson due to contamination of the charm daughters, and S_{det} and S^{det}_{tail} are the global scaling factors due to the systematic uncertainties in the vertex resolutions (σ_z^{CP} and σ_z^{tag}) computed from the track helix errors in the vertex fits. We find the S_{charm} and S^{charm}_{tail} to be $S_{charm} = 0.42^{+0.08}_{-0.09}$ and

$S_{tail}^{charm} = 0.0^{+1.1}_{-0.0}$ from the Monte Carlo simulation studies. The S_{det} and S_{tail}^{det} must be determined from the data as they depend on the detector performance. S_{det} is determined using a $D^0 \to K^-\pi^+$ sample. The production vertex of the the D^0 is measured using the primary tracks in the same hemisphere as the D^0 candidate with the IP constraint. The distance between the D^0 decay vertex and the production vertex in the z direction is fit using the same resolution function and known D^0 lifetime to obtain S_{det}. We find $S_{det} = 1.00 \pm 0.03$ for the data and $S_{det} = 1.23 \pm 0.02$ from the Monte Carlo simulation studies of the D^0 sample. As we find $S_{det} = 1.16 \pm 0.03$ for $B \to J/\psi K$ Monte Carlo sample, we scale the S_{det} to be $S_{det} = (1.00 \pm 0.03) \cdot (1.16 \pm 0.03)/(1.23 \pm 0.02) = 0.94 \pm 0.04$. S_{tail}^{det} is determined to be 2.4 ± 0.6 in the measurement of the B lifetime using the $B \to \bar{D}^* \ell^+ \nu$ sample.

A small fraction of events have large reduced χ^2s. We find that the errors of the vertices computed from the errors of the track helix parameters in the vertex fits underestimate the vertex resolution and in fact, that the vertices with large χ^2s have worse resolution than those estimated. In order to take into account this effect, we introduce the effective vertex resolutions $\tilde{\sigma}_z^{CP}$ and $\tilde{\sigma}_z^{tag}$ when χ^2/ndf is greater than 3:

$$\begin{aligned}
(\tilde{\sigma}_z^{CP})^2 &\equiv [1 + \alpha_{CP}\{(\chi^2/ndf)_{CP} - 3\}](\sigma_z^{CP})^2 : \ (\chi^2/ndf)_{CP} > 3, \\
(\tilde{\sigma}_z^{tag})^2 &\equiv [1 + \alpha_{tag}\{(\chi^2/ndf)_{tag} - 3\}](\sigma_z^{tag})^2 : \ (\chi^2/ndf)_{tag} > 3,
\end{aligned}$$

where $(\chi^2/ndf)_{CP}$ and $(\chi^2/ndf)_{tag}$ are the reduced χ^2 of the vertex fits for the CP- and tag-side B decay vertices, respectively.

As mentioned above, $\mu_{\Delta t}$ (and $\mu_{tail}^{\Delta t}$) originates from the shift of the mean of the Δz measurements, $\mu_{\Delta z}$ (and $\mu_{tail}^{\Delta z}$):

$$\begin{aligned}
\mu_{\Delta t} &\equiv \frac{\mu_{\Delta z}}{c(\beta\gamma)}, \\
\mu_{tail}^{\Delta t} &\equiv \frac{\mu_{tail}^{\Delta z}}{c(\beta\gamma)}.
\end{aligned}$$

This shift of the Δz, $\mu_{\Delta z}$ and $\mu_{tail}^{\Delta z}$, is caused by the contamination of the charm daughters in the vertex reconstruction of the tagging side B meson and is correlated with the σ_z^{tag}:

$$\begin{aligned}
\mu_{\Delta z}(\sigma_z^{tag}) &= \mu_0 + \alpha_\mu \sigma_z^{tag}, \\
\mu_{tail}^{\Delta z}(\sigma_z^{tag}) &= \mu_{tail}^0 + \alpha_{tail}^{\mu} \sigma_z^{tag}.
\end{aligned}$$

The μ_0 and α_μ are determined to be $\mu_0 = -6 \pm 4$ μm and $\alpha_\mu = -0.17 \pm 0.06$ using the Monte Carlo simulation. Since α^{μ}_{tail} is found to be consistent with zero, $\mu^{\Delta z}_{tail}$ is fixed at the value -160 μm determined from the Monte Carlo simulation studies.

Figure 6 shows the sum of event-by-event resolution functions described above, over 300 $B^\pm \to J/\psi K^\pm$ events. The width of this distribution is dominated by the main Gaussian ($1 - f_{tail} = 0.96 \pm 0.04$); we find $\bar{\sigma} \approx 1.11$ ps, $\bar{\sigma}_{tail} \approx 2.24$ ps and $\bar{\mu} = -0.19$ ps, where "–" indicates the average over all events. The μ_{tail} is fixed to -1.25 ps based on the Monte Carlo simulation studies.

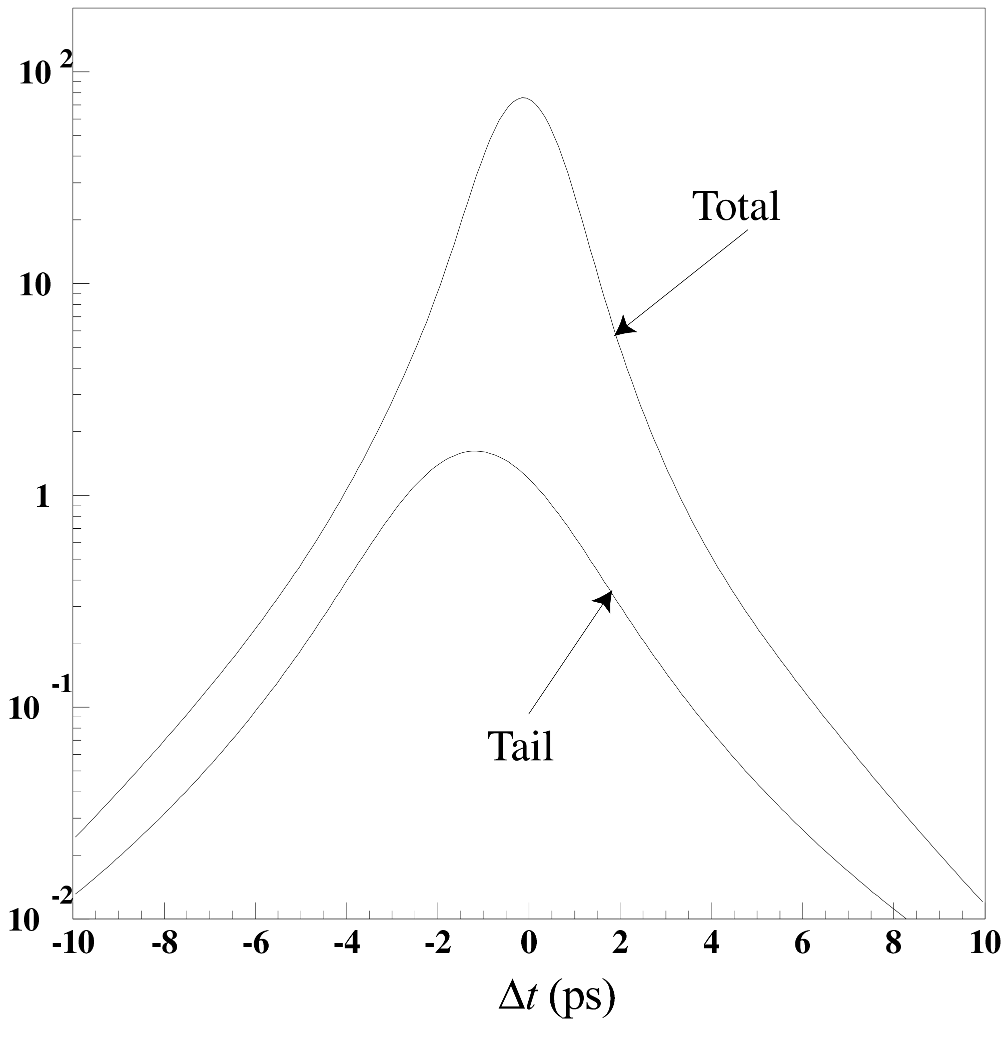

Fig. 6. The sum of event-by-event resolution functions of over 300 $B^\pm \to J/\psi K^\pm$ events, showing the average shape of the resolution function.

3.3.2 Measurements of B lifetimes

Using the vertex reconstruction algorithm and the resolution function described in the previous sections, we measure lifetimes of neutral and charged B mesons. Figures 7 and 8 show Δt distributions of decay modes that involve J/ψ with the result of the fit. Table 5 summarizes the results. The results for different decay modes of the B are consistent with each other and are in good agreement with the world average.

Table 5. Summary of B meson lifetime measurements

Decay mode	Lifetime (ps)
$\bar{B}^0 \to D^{*+}\ell^-\nu$	$1.50 \pm 0.06^{+0.06}_{-0.04}$
$\bar{B}^0 \to D^{*+}\pi^-$	$1.55^{+0.18}_{-0.17}{}^{+0.10}_{-0.07}$
$\bar{B}^0 \to D^{+}\pi^-$	$1.41^{+0.13}_{-0.12} \pm 0.07$
$\bar{B}^0 \to J/\psi\bar{K}^{*0}$	$1.56^{+0.22}_{-0.19}{}^{+0.09}_{-0.15}$
Combined	$1.50 \pm 0.05 \pm 0.07$
$\bar{B}^0 \to J/\psi K_S$	$1.54^{+0.28}_{-0.24}{}^{+0.11}_{-0.19}$
$\bar{B}^0 \to J/\psi K_L$	$1.28^{+0.36}_{-0.35}$
$B^- \to D^{*0}\ell^-\nu$	$1.54 \pm 0.10^{+0.14}_{-0.07}$
$B^- \to D^0\pi^-$	$1.73 \pm 0.10 \pm 0.09$
$B^- \to J/\psi K^-$	$1.87^{+0.13}_{-0.12}{}^{+0.07}_{-0.14}$
Combined	$1.70 \pm 0.06^{+0.11}_{-0.10}$

3.4 Maximum likelihood

An unbinned maximum likelihood method is used to extract the best value for $\sin 2\phi_1$. The probability density function expected for the signal distribution with a CP eigenvalue of η_f is given by:

$$Sig(\Delta t, \eta_f, q) = \frac{1}{\tau_{B^0}} \exp(-|\Delta t|/\tau_{B^0}) \times (1 - q(1-2\omega)\eta_f \sin 2\phi_1 \sin(\Delta m_d \Delta t))$$

where $q = 1(-1)$ if the tag is $B^0(\bar{B}^0)$ and ω depends on the flavor tagging method as given in the previous section. The values of τ_{B^0} and Δm_d are fixed to the world averages,1.548 ± 0.032 ps and 0.472 ± 0.017 ps^{-1}, respectively. By investigating events in background dominated regions (the side bands in the ΔE and

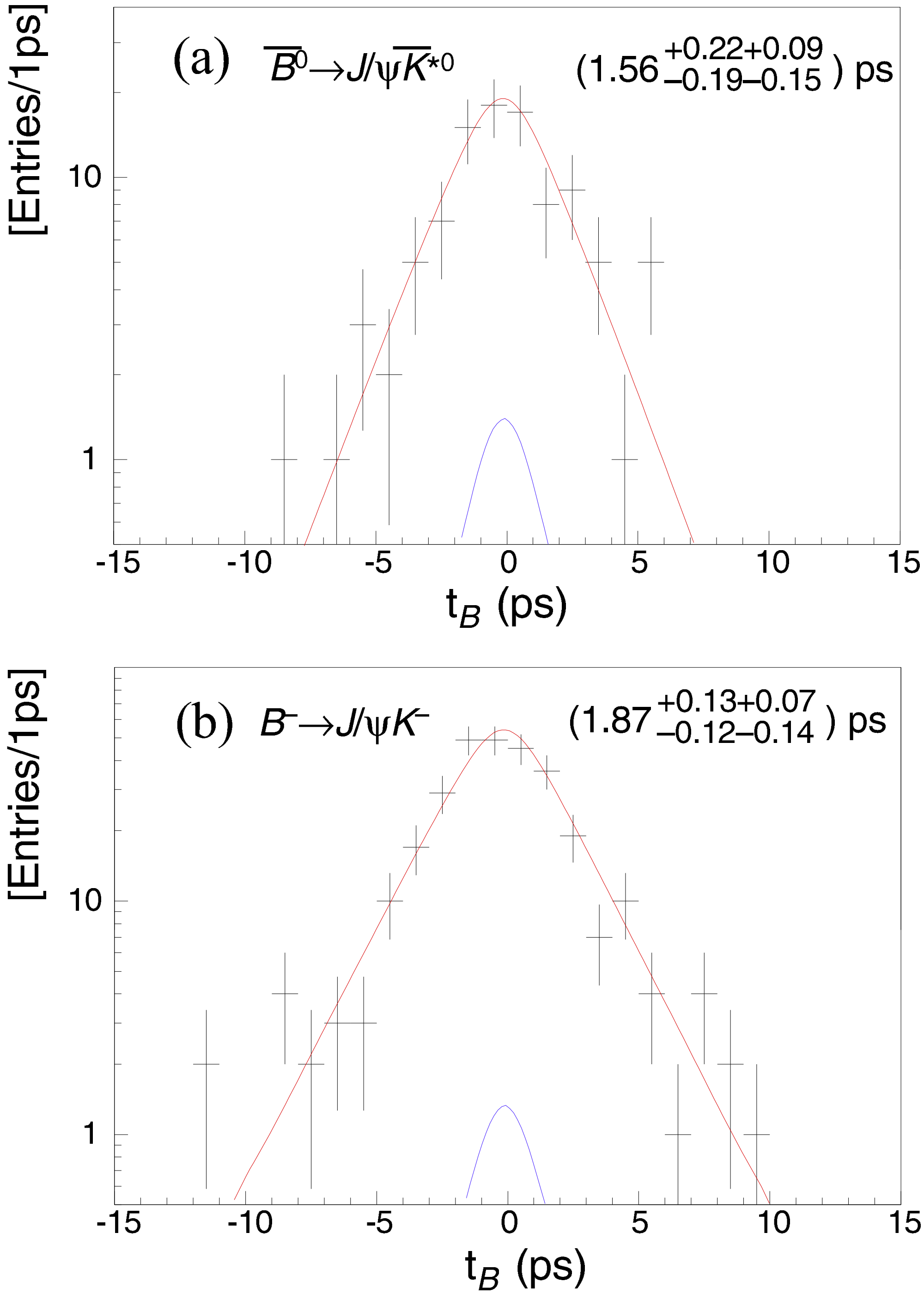

Fig. 7. Δt distributions and the results of the fit for (a) $\bar{B}^0 \to J/\psi \bar{K}^{*0}$, (b) $B^- \to J/\psi K^-$. The lower solid curve represents the background distribution.

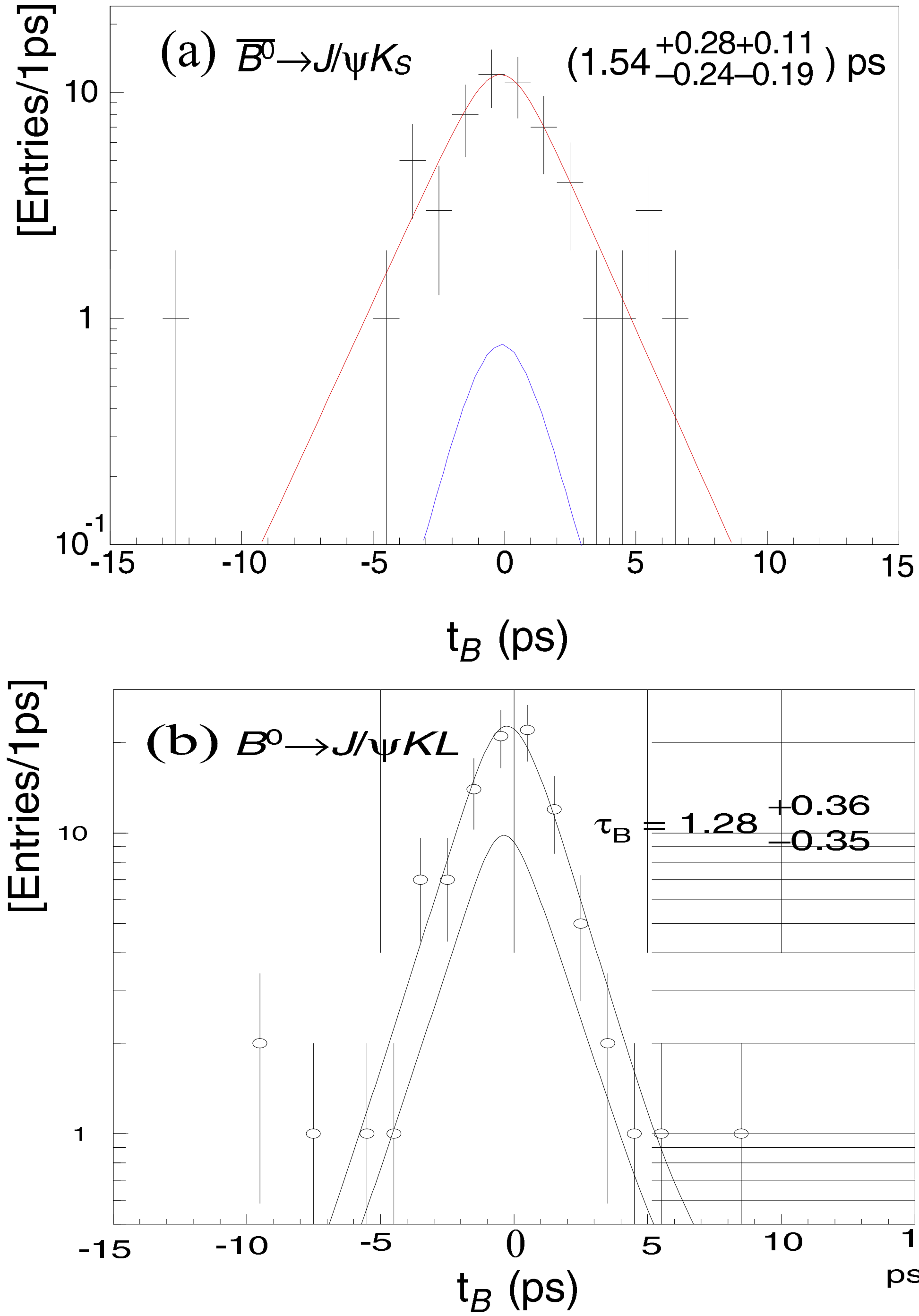

Fig. 8. Δt distributions and the results of the fit for (a) $\bar{B}^0 \to J/\psi K_S$, (b) $\bar{B}^0 \to J/\psi K_L$. The lower solid curve represents the background distribution.

M_{beam} two dimensional plots), we find that the probability density function for the background events is consistent with

$$Bkg(\Delta t) = \frac{1}{2\tau_{bkg}} \exp(-|\Delta t|/\tau_{bkg})$$

where $\tau_{bkg} = 0.73 \pm 0.12$ ps, except for the case of $B^0 \to J/\psi K_L$ candidates. The likelihood of an event, $\imath$, is calculated as:

$$\rho_i = p_{sig} \int_{-\infty}^{+\infty} Sig(s, \eta_f, q) R(\Delta t - s) ds + (1 - p_{sig}) \int_{-\infty}^{+\infty} Bkg(s, \eta_f, q) R(\Delta t - s) ds$$

where p_{sig} is the probability for the event being a signal, and $R(\Delta t)$ is the resolution function described in the previous section. The log-likelihood, $-\sum_i ln\rho_i$ is calculated by summing over all candidate events. The most probable $\sin 2\phi_1$ value is found by scanning over $\sin 2\phi_1$ values to minimize the log likelihood function.

We perform a simultaneous fit to $CP = -1$ and $CP = +1$ candidate events to extract the $\sin 2\phi_1$ value. Figure 9(a) shows the log-likelihood as a function of $\sin 2\phi_1$ for a total of 98 $CP = -1$ and $CP = +1$ candidate events. The log-likelihood for $CP = -1$ and $CP = +1$ events are shown separately. We find $\sin 2\phi_1 = 0.45^{+0.43}_{-0.44}$. To display the results of the fit, $dN/d(\Delta t)$ for $q = +1$ and $dN/d(-\Delta t)$ for $q = -1$ for $\eta_f = -1$ and $dN/d(-\Delta t)$ for $q = +1$ and $dN/d(\Delta t)$ for $q = -1$ for $\eta_f = +1$ are combined so that the distribution becomes approximately proportional to $\exp(-|\Delta t|/\tau_{B^0})(1 + (1 - 2\omega) \sin 2\phi_1 \sin(\Delta m_d \Delta t))$, as shown in Figure 9(b).

The results of the fit to the tagged events of various CP modes are summarized in Table 6. To display the fitted results, the $dN/d\Delta t$ distribution for $q = +1$ events and $dN/d(-\Delta t)$, $q = -1$ are added. Figure 10(a) and (b) show the results for only $J/\psi K_S, K_S \to \pi^+\pi^-$ events and for all $CP = -1$ events combined. Figure 11 shows the results for $CP = +1$ events, *i.e.* $J/\psi K_L$ and $J/\psi \pi^0$. In fitting to $J/\psi K_L$ candidate events, the background due to $J/\psi K_L \pi^0$, which amounts to $\approx$ 17% of the total background, is taken to be a mixture of $CP = -1(73\%)$ and $CP = +1(27\%)$ states, based on the results of a $B \to J/\psi K_S \pi^0$ analysis. A fit to 52 events in the $J/\psi K_L$ sideband ($1.0 > p_B^* > 2.0$ GeV/c region), where the non-CP $J/\psi X$ events dominate, gives the result, $\sin 2\phi_1 = 0.02^{+0.48}_{-0.49}$, consistent with null asymmetry.

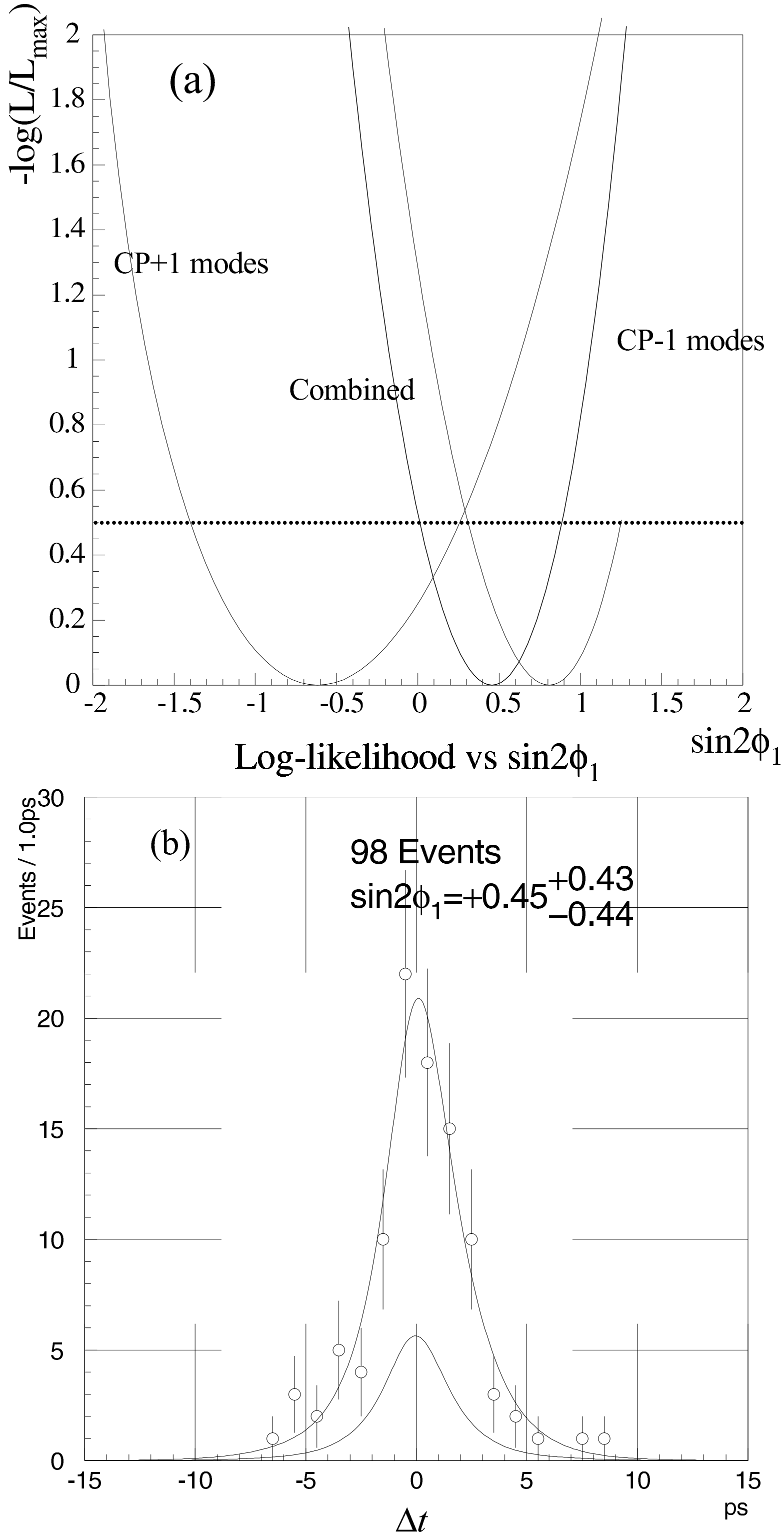

Fig. 9. (a) The log likelihood as a function of $\sin 2\phi_1$. (b) a sum of $dN/d(\Delta t)$ for $q = +1$ and $dN/d(-\Delta t)$ for $q = -1$ for $\eta_f = -1$ and $dN/d(-\Delta t)$ for $q = +1$ and $dN/d(\Delta t)$ for $q = -1$ for $\eta_f = +1$ events with the result of the fit. The lower solid curve represents the background distribution.

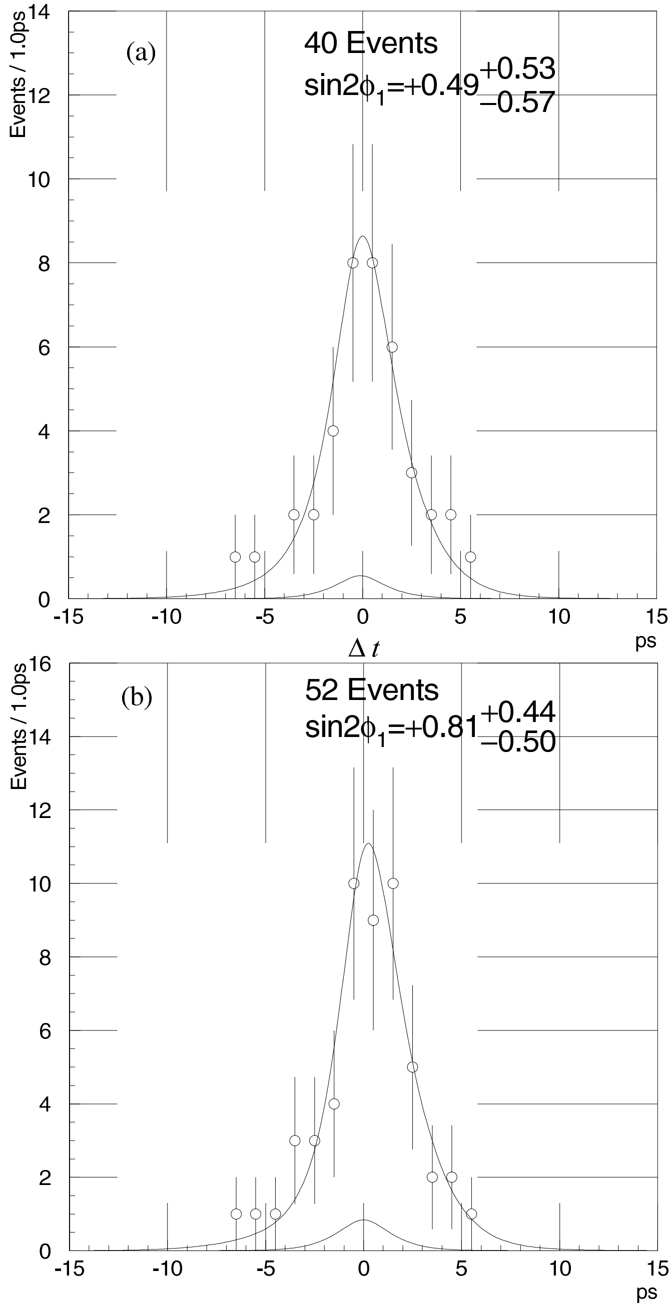

Fig. 10. Sum of $dN/d(\Delta t)$ for $q = +1$ and $dN/d(-\Delta t)$ for $q = -1$ for $\eta_f = -1$ events with the results of the fit for (a) $B^0 \to J/\psi K_S$, $K_S \to \pi^+\pi^-$ mode and (b) all $CP = -1$ modes combined. The lower solid curves represent the background distribution.

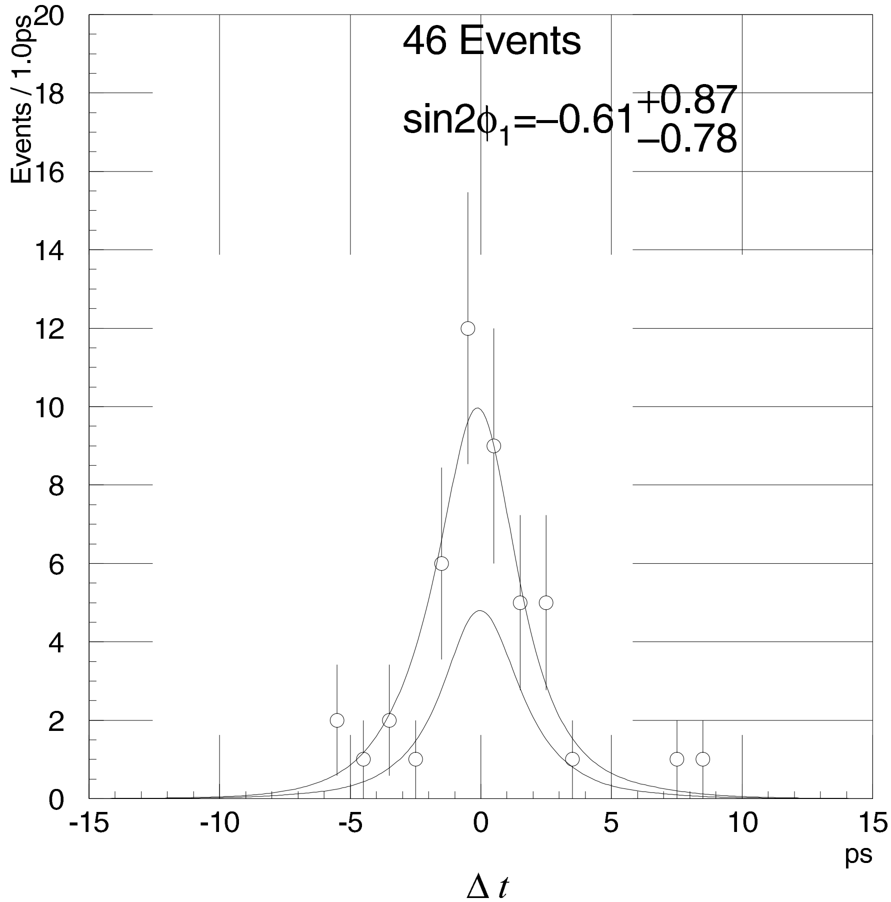

Fig. 11. Sum of $dN/d(\Delta t)$ for $q = +1$ and $dN/d(-\Delta t)$ for $q = -1$ for $\eta_f = -1$ events with the results of the fit for all $CP = +1$ modes combined. The lower solid curves represent the background distribution.

Table 6. Summary of CP fits to tagged CP events.

Category	$\sin 2\phi_1$
$J/\psi K_S, K_S \to \pi^+\pi^-$	$0.49^{+0.53}_{-0.57}$
All $CP = -1$ modes combined	$0.81^{+0.44}_{-0.50}$
All $CP = +1$ modes combined	$-0.61^{+0.87}_{-0.78}$
All modes combined	$0.45^{+0.43}_{-0.45}$

3.4.1 Systematic checks

To test for possible bias in the analysis, we apply the same analysis procedure including tagging, vertexing and log-likelihood fitting to control data samples with null intrinsic CP asymmetry; $B^0 \to J/\psi K^{*0}, K^{*0} \to K^+\pi^-$, $B^- \to J/\psi K^-$, $B^- \to D^0\pi^-$, and $B^0 \to D^{*-}\ell^+\nu$ decays. Figures 12 and 13 show the Δt distributions for $B^0 \to J/\psi K^{*0}, K^{*0} \to K^+\pi^-$, $B^- \to J/\psi K^-$, and $B^- \to D^0\pi^-$ events. The results of the fit for these samples are given in Table 7. All results are consistent with the null asymmetry.

Table 7. Summary of CP fits to control samples.

Category	Fit results
$\bar{B}^0 \to J/\psi \bar{K}^{*0}, \bar{K}^{*0} \to K^-\pi^+$	$-0.09^{+0.49}_{-0.46}$
$B^- \to J/\psi K^-$	$0.22^{+0.23}_{-0.24}$
$B^- \to D^0\pi^-$	-0.10 ± 0.17
$\bar{B}^0 \to D^{*+}\ell^-\bar{\nu}$	0.09 ± 0.18

We generate 1000 toy Monte Carlo experiments with the same number of tagged CP events, having the same composition of the tags and the same resolutions as in the CP data sample, for an input value of $\sin 2\phi_1 = 0.45$. Figure 14(a) and (b) show the distributions of the central $\sin 2\phi_1$ value and the statistical errors, the + side and − side separately. We find that the probability of obtaining a value of the statistical error greater than the values observed is $\approx 5\%$.

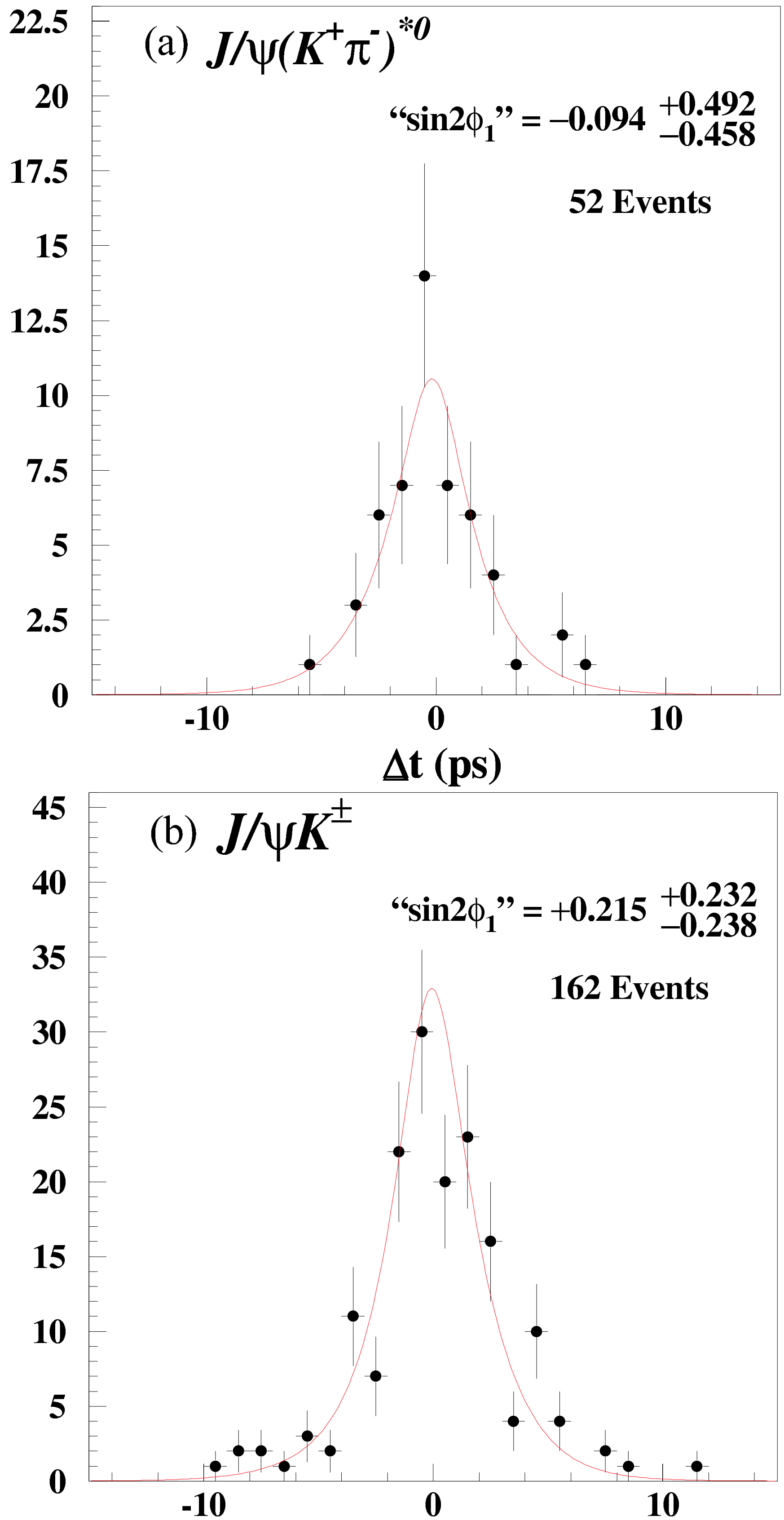

Fig. 12. Δt distributions for (a) $B^0 \to J/\psi K^{*0}$, $K^{*0} \to K^+\pi^-$ and (b) $B^- \to J/\psi K^-$ events.

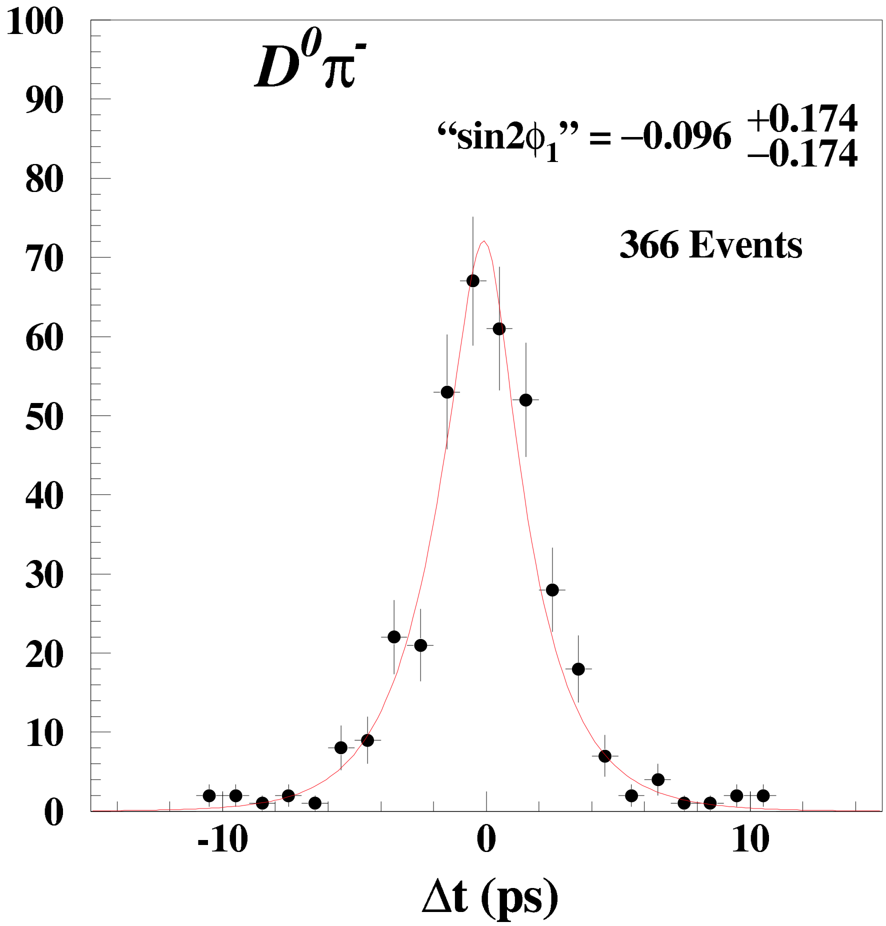

Fig. 13. Δt distributions for $B^- \to D^0\pi^-$ events.

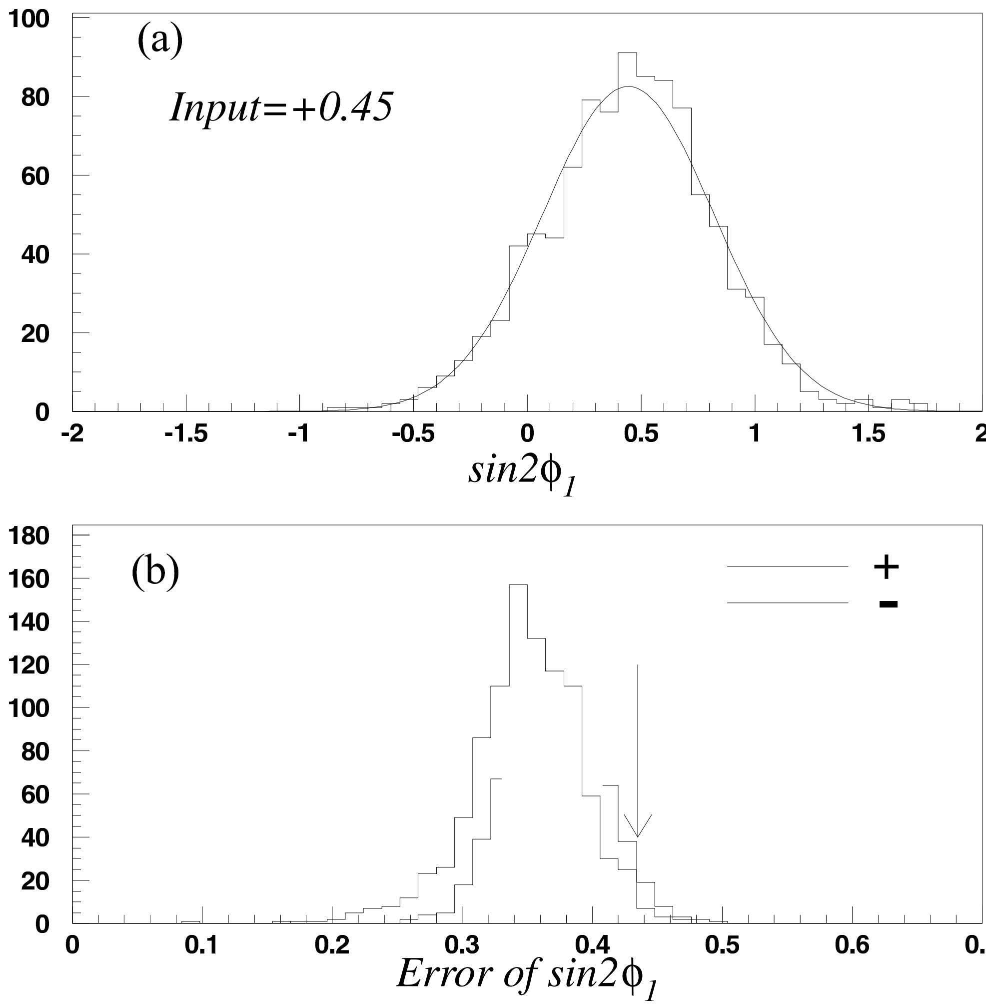

Fig. 14. Results of 1000 toy Monte Carlo experiments generated for $\sin 2\phi_1 = 0.45$. (a) the distribution of the fitted values of $\sin 2\phi_1$ is shown as the histogram with a fit to a Gaussian. (b) the distribution of the fitted errors on the $+$ side and $-$ side are shown separately.

3.4.2 Systematic errors

Table 8 summarizes the systematic errors. The largest source of systematic errors is the uncertainty in the wrong-tag fraction determination. The effect of this error is studied by varying the value of ω individually for each tagging method. The effect due to uncertainty in Δt resolutions for both signal and background is studied by varying parameters in the resolution function, $R(\Delta t)$. Also included are the effects due to uncertainties in the estimates of the background fraction, in the world average τ_{B^0} and Δm_d values. An imperfect knowledge of the event by event interaction point could cause a systematic error in $\sin 2\phi_1$ due to the vertex reconstruction. This effect is studied by repeating the entire fitting procedure by varying the IP envelope by $\pm 1\sigma$ in all three dimensions. The total systematic error of $\sin 2\phi_1$ is found to be $+0.07$ and -0.09.

Table 8. List of systematic errors of $\sin 2\phi_1$

Source	σ(+ side)	σ(− side)
Wrong-tag	0.050	0.066
$R(\Delta t)$	0.026	0.025
Background shape	0.029	0.042
Background fraction	0.029	0.032
$\tau_{B^0}, \Delta m_d$	0.005	0.005
IP profile	0.004	0.000
Total	0.07	0.09

4 Conclusions

Using 98 flavor tagged events, we made a preliminary measurement of the time-dependent CP asymmetry in B^0 decays into CP eigenstates: $J/\psi K_S, K_S \to \pi^+\pi^-$ and $K_S \to \pi^0\pi^0$; $\psi(2S)K_S, K_S \to \pi^+\pi^-$; $\chi_{c1}K_S, K_S \to \pi^+\pi^-$; $J/\psi\pi^0$; and $J/\psi K_L$. We find $\sin 2\phi_1 = 0.45^{+0.43}_{-0.44}(stat)^{+0.07}_{-0.09}(syst)$.

Figure 15 shows the constraint on the angle ϕ_1 corresponding to this measurement, $\sin 2\phi_1 = 0.45^{+0.44}_{-0.45}$, together with the constraints derived from other measurements. While the current statistical uncertainty of our measurement does not allow anything conclusive, the result is consistent with the Standard Model prediction.

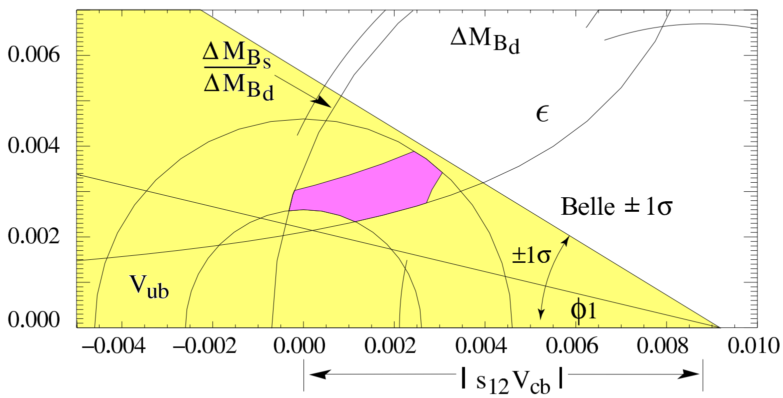

Fig. 15. Constraint on the angle ϕ_1 corresponding to this measurement $\pm 1\sigma$, $\sin 2\phi_1 = 0.45^{+0.44}_{-0.45}$. This figure was made from Fig. 11.2 of Ref. [7] .

5 Acknowledgments

We gratefully acknowledge the efforts of the KEKB group in providing us with excellent luminosity and running conditions and the help with our computing and network systems provided by members of the KEK computing research center. We thank the staffs of KEK and collaborating institutions for their contributions to this work, and acknowledge support from the Ministry of Education, Science, Sports and Culture of Japan and the Japan Society for the Promotion of Science; the Australian Research Council and the Australian Department of Industry, Science and Resources; the Department of Science and Technology of India; the BK21 program of the Ministry of Education of Korea and the Basic Science program of the Korea Science and Engineering Foundation; the Polish State Committee for Scientific Research under contract No.2P03B 17017; the Ministry of Science and Technology of Russian Federation; the National Science Council and the Ministry of Education of Taiwan; the Japan-Taiwan Cooperative Program of the Interchange Association; and the U.S. Department of Energy.

References

[1] J.H. Christenson et al., Phys Rev. Lett. **13**, 138 (1964).

[2] M. Kobayashi and T. Maskawa, Prog. Theo. Phys. **49**, 652 (1973).

[3] A. Carter and A.I. Sanda, Phys. Rev. Lett. **45**, 952 (1980);
A. Carter and A.I. Sanda, Phys. Rev. **D23**, 1567 (1981);
I.I. Bigi and A.I. Sanda, Nucl. Phys. **B193**, 851 (1981).

[4] P. Oddone, in Proceedings of *the UCLA Workshop: Linear Collider $B\overline{B}$ Factory Conceptual Design*, D. Stork, ed., World Scientific, p. 243 (1987).

[5] "KEKB B-Factory Design Report", KEK Report 95-7 (1995);
K. Akai, et al., "COMMISSIONING OF THE KEKB B-FACTORY", WEAR4, Proc. 1999 Particle Accelerator Conference, New York (1999);
K. Akai, et al., "COMMISSIONING OF THE KEKB B-FACTORY", Proc. Intl. Workshop on e^+e^- Factories, Tsukuba, Japan, edited by K. Akai and E. Kikutani (1999);
H. Fukuma, et al., "OBSERVATION OF VERTICAL BEAM BLOW-UP IN KEKB LOW ENERGY RING", Proc. 2000 European Particle Accelerator Conference, Vienna (2000);
Y. Funakoshi, et al., "KEKB PERFORMANCE", Proc. 2000 European Particle Accelerator Conference, Vienna (2000).

[6] Belle Collaboration, *The Belle Detector*, Submitted to Nucl. Instrum. Methods (2000).

[7] Particle Data Group, D.E. Groom, et al., Eur. Phys. J. **C15**, 1 (2000).